ELSEVIER

Journal of Molecular Catalysis A: Chemical 162 (2000) 33–50

JOURNAL OF MOLECULAR CATALYSIS A: CHEMICAL

www.elsevier.com/locate/molcata

Structure–reactivity correlations for oxide-supported metal catalysts: new perspectives from STM

Xiaofeng Lai, D. Wayne Goodman *

Department of Chemistry, Texas A&M University, P.O. Box 30012, College Station, TX 77842-3012, USA

Abstract

Deposition of metals onto planar oxide supports provides a convenient methodology for modeling important aspects of supported metal catalysts. In this work, scanning tunneling microscopy (STM), in conjunction with traditional surface-science techniques, is used to monitor the morphological changes of oxide-supported metal clusters upon exposure to reactants at elevated pressures. Of special concern is the relationship between catalytic activity/selectivity and surface structure, e.g., metal–support interaction and intrinsic cluster size effects. Au and Ag clusters were vapor-deposited onto $TiO_2(110)$ under ultrahigh vacuum (UHV) conditions. Characterization of cluster size and density as a function of metal coverage is correlated with catalytic reactivity. Oxygen-induced cluster ripening occurs upon exposure of $Au/TiO_2(110)$ and $Ag/TiO_2(110)$ to 10.00 Torr O_2. The morphology of the metal clustering induced by O_2 exposure implies the chemisorption of O_2 onto the metal clusters and the TiO_2 substrate at room temperature. Ag and Au clusters exhibited a bimodal size distribution following O_2 exposure due to Ostwald ripening, i.e., some clusters increased in size while other clusters shrank. A volatile oxide species is proposed to form at high oxygen pressures, accelerating intercluster atom transport. The oxide substrate was found to play a role in the kinetics of cluster ripening. STM shows that oxide-supported metal clusters are very reactive to O_2 and that nanoclusters are particularly susceptible to adsorbate-induced restructuring.

Keywords: Supported metal catalysts; STM; UHV

1. Introduction

The metal/oxide interface has received considerable attention due to its importance in a range of technologies, particularly catalysis. Substantial efforts have focused on the chemical and physical properties of supported metal clusters and their interactions with oxide supports [1–3]. A common goal of catalytic research is defining the relationship between catalytic activity/selectivity and surface structure. In particular, for oxide-supported metals, key issues are intrinsic cluster-size effects and metal–support interactions. Advances in the last 30 years of ultrahigh vacuum (UHV) surface-science methodology allow the study of surfaces at the atomic level. An integrated approach that combines these modern surface techniques with traditional experimental methodologies can provide valuable new insights into a wide range of catalytic phenomena.

The discovery of the photocatalytic activity of TiO_2 electrodes [4] for water decomposition has

* Corresponding author. Tel.: +1-979-845-0214; fax: +1-979-845-6822.

E-mail address: goodman@mail.chem.tamu.edu (D.W. Goodman).

1381-1169/00/$ - see front matter
PII: S1381-1169(00)00320-4

promoted extensive studies of TiO_2 and its interaction with supported metal clusters. Scanning tunneling microscopy (STM) has been used for the structural studies of TiO_2 surfaces at the atomic scale related to oxygen vacancies and reconstruction [5–30]. For chemisorption studies on metal/TiO_2 systems, much of the work has focused on the effect of TiO_2 surface defects on adsorption and dissociation of adsorbates such as CO, O_2, H_2, H_2O, etc. [31–47]. For example, dissociative adsorption of H_2O and H_2 increases the number of oxygen defects on the nearly perfect surface. Using low-energy electron diffraction (LEED), X-ray photoelectron spectroscopy (XPS), electron-energy-loss spectroscopy (EELS) and temperature-programmed desorption (TPD), Göpel et al. [39] have shown that surface defects are thermodynamically stable at high temperatures and act as donors and specific adsorption sites for H_2 and CO.

For "real world" catalysts, which often consist of small metal clusters supported on oxide substrates, changes associated with the substrate and the supported metal clusters are of equal importance. The density and the size of the metal clusters can be carefully controlled by depositing metals onto clean oxide single crystals or thin films. The morphology of the metal clusters, however, can depend on the preparation conditions and subsequent treatment of the model catalysts. Therefore, characterization of the clusters before, during and after catalytic reactions is essential.

Previous studies have used an array of surface spectroscopies to study catalytic reaction mechanisms; however, STM has been used less frequently for the direct imaging of structural changes at the metal/oxide interface. Recently, Berkó et al. [48–52], using STM, reported that exposures of CO between 10^{-3} and 10^{-1} mbar to Rh/TiO_2(110)–(1×2) led to significant agglomeration of the Rh clusters [48–51]. This agglomeration was attributed to the formation of Rh–CO bonds (185 kJ mol^{-1}) that promoted disruption of the weaker Rh–Rh bonds (44.5 kJ mol^{-1}). Similar observations have been made for Ir/TiO_2(110)–(1×2) [52].

The physical and chemical properties of small, supported metal clusters (<100 nm) are known to be markedly size dependent [53]. Nano-sized Au clusters supported by an oxide support are active for a number of catalytic reactions such as low-temperature CO oxidation, NO reduction, hydrogenation and partial oxidation of hydrocarbons [54–75]. These discoveries have prompted extensive studies of the catalytic properties of supported Au. Haruta et al. [55,58–63,69–72,74] have demonstrated that the catalytic properties of Au depend on the choice of the oxide support, the preparation methods, and in particular, the size of the Au clusters. However, despite considerable effort, no consensus exists regarding the mechanism responsible for the unique structure sensitivity of Au nanoclusters.

This paper summarizes our recent STM studies of Au and Ag clusters supported on TiO_2. New concepts and insights into the surface chemistry of the metal/oxide interface are highlighted. Morphological changes of model catalysts induced by surface reactions at elevated pressures are examined and an Ostwald ripening mechanism is proposed. This work illustrates that the limited dimensionality of the metal clusters and the properties of the oxide support play significant roles in altering the catalytic activity of supported metal clusters.

2. Experimental

The experiments were performed in two UHV systems. The first was a combined elevated-pressure reactor/multi-technique UHV analysis chamber (base pressure, $\sim 1.0\times10^{-10}$ Torr) equipped with a double-pass cylindrical mirror analyzer for Auger electron spectroscopy (AES) and XPS, LEED optics (Perkin-Elmer), quadrupole mass spectrometer (QMS) and a UHV STM (Omicron); and an elevated-pressure reactor, isolated from the main chamber by a gate valve, for the reaction studies. Following preparation and characterization in the primary UHV chamber, the sample was transferred in situ into the elevated-pressure reactor via a differentially pumped Teflon sliding seal. This design provides a convenient way of carrying out high-pressure adsorption and reaction studies in the 10^{-8}–10^{3} Torr range, while maintaining UHV conditions in the main chamber.

The kinetics studies were carried out in a second UHV chamber (base pressure, $\sim 6.0\times10^{-10}$ Torr) equipped with AES, TPD and a contiguous high-

pressure reactor. The reaction products were extracted from the reactor with a vacuum syringe, the gas mixture compressed, then injected into a gas chromatograph (GC).

In this study, Au and Ag clusters with diameters between 1.0 and 7.0 nm were grown by vapor deposition onto a TiO_2 surface. The average metal-cluster size varies with metal flux, deposition time, total dose, and substrate temperature [76,77]. The Ag and Au dosers were constructed of high-purity wires of the parent metal wrapped around a W wire (0.010 in. diameter, H&R Cross) and extensively outgassed prior to use. The flux of each metal doser was calibrated via AES of the corresponding metal deposited onto Re(0001) and its coverage verified with STM. Metal coverages are reported in monolayers (ML), where 1.0 ML corresponds to $\sim 1.4 \times 10^{15}$ atoms/cm^2.

A W-5%Re/W-26%Re thermocouple was attached to the edge of the TiO_2 crystal using a high-temperature ceramic adhesive (AREMCO 571). The thermocouple was used to measure the surface temperature and to calibrate a remote pyrometer (OMEGA OS3700). Subsequent to the removal of the thermocouple for sample transfer, the pyrometer was used to measure the sample temperature. The emissivity of TiO_2 was assumed to be 0.50 [78].

3. Results and discussion

3.1. Surface characterization of metal / TiO_2(110)

The morphology of the TiO_2(110) surface depends markedly on the conditions of the sample preparation. Generally, cycles of Ar^+ bombardment and subsequent annealing to 1000–1150 K produce a (1×1) surface with extensive, relatively flat terraces [76,77]. The top image of Fig. 1 shows the TiO_2(110)–(1×1) surface annealed to 1100 K, with individual atom rows evident along the [001] direction of the terraces. The spacing of the rows is ~ 6.5 Å, corresponding to the length of the unit cell along the $[1\bar{1}0]$ direction for the unreconstructed TiO_2(110) surface. The bright rows, following the assignment of Onishi et al. [5–7], are identified as five-fold coordinated Ti^{4+} sites and the dark rows correspond to the bridging oxygen rows. The flat terraces are separated by mono-atomic steps, with some small, irregular clusters (presumably TiO_2) evident along the step edges.

An extended view of the surface morphology of the Au/TiO_2(110) surface, an $(150 \times 150\ nm^2)$ STM image of 1.0 ML Au/TiO_2, is shown in the bottom image of Fig. 1. Hemispherical clusters with a narrow size distribution grow preferentially along the step edges with clusters on the flat terraces evident as well [77]. At an Au coverage of 1.0 ML, more than 60% of the substrate is still metal-free and separated by mono-atomic steps, consistent with 3D clustering or a Volmer–Weber (VW) growth mode of Au on TiO_2(110), and in agreement with a previous work based on ISS [79]. The island growth mode has been frequently observed for other transition metals on oxide supports, including Pd [76], Ag [80], Ni [81], Rh [48], Ir [52], etc.

The growth of the cluster size and density was studied as a function of metal coverage. For example, with increasing Au coverage, the average cluster size (diameter) increased from 2.0 nm for 0.10 ML Au to 5.4 nm for 4.0 ML Au (Fig. 2). However, a rapid increase in cluster density was observed upon deposition of 0.10 ML Au while the cluster density remained essentially constant at higher Au coverages > 1.0 ML. With an increase in the Au coverage from 0.10 to 0.25 ML, the cluster density increased by $\sim 30\%$, with a further increase of $\sim 50\%$ from 0.25 to 1.0 ML Au. The cluster density reached a maximum at ~ 2.0 ML, where $\sim 70\%$ of the substrate surface was covered by Au clusters. At higher Au coverages, the cluster density declined due to cluster coalescence and agglomeration. Approximately 60% of the nucleating sites were populated at a coverage of 0.25 ML [77].

The cluster size, in contrast to cluster density, increased continuously with Au coverage. Increasing the Au deposition from 0.10 to 2.0 ML increased the cluster size from 2.0 to 4.5 nm. A rapid increase in Au cluster size occurred for very low Au coverages (below 0.10 ML). Higher Au coverages correlated with a decline in cluster growth. It is noteworthy that the increase in cluster volume was not proportional to the increase in cluster size. For example, a 22% increase in the average cluster diameter, from 3.7 nm (1.0 ML) to 4.5 nm (2.0 ML), corresponds to an 80%

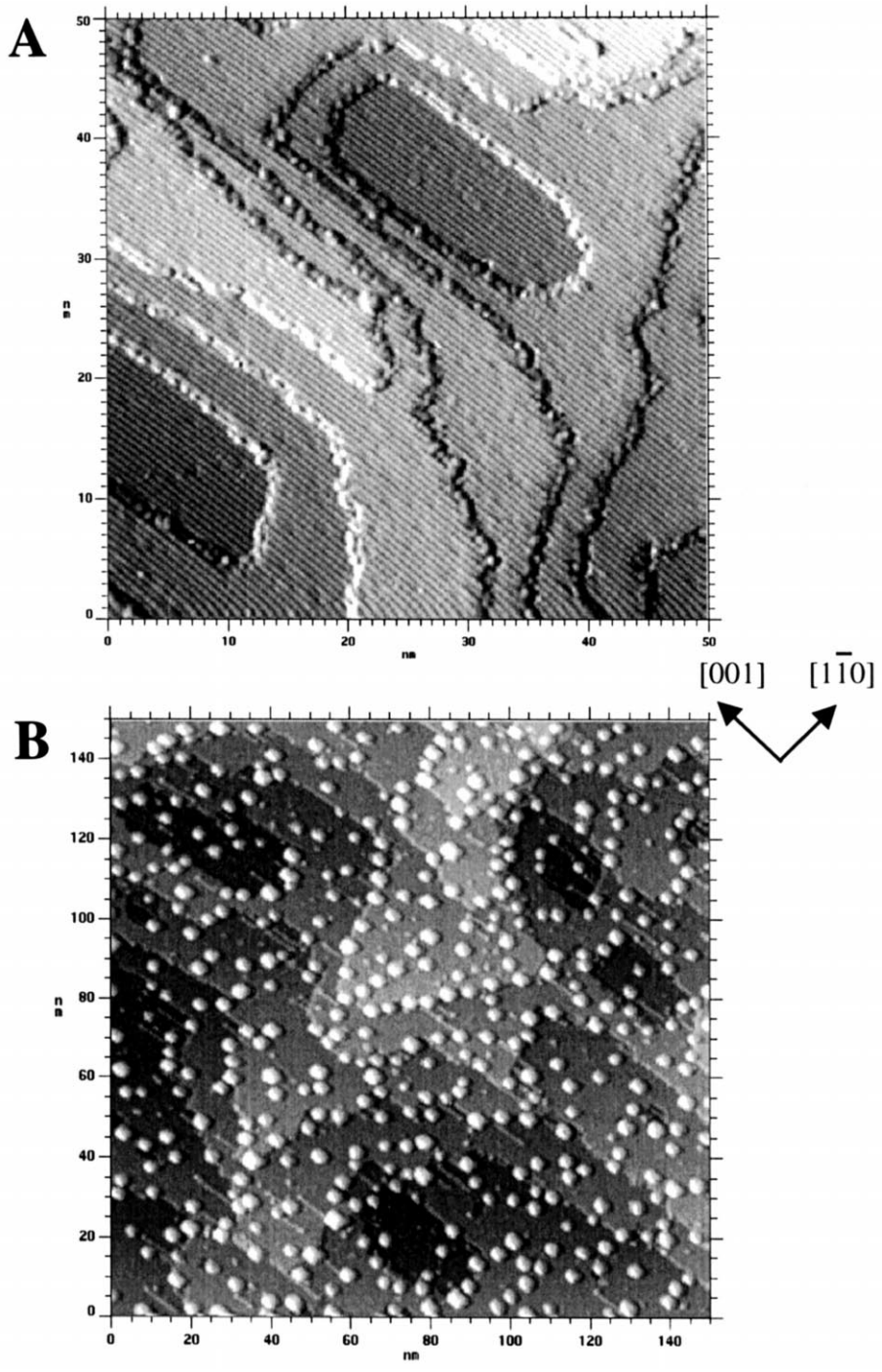

Fig. 1. Top: an STM image (2.0 V, 2.0 nA) of the TiO_2(110) surface acquired after cycles of sputtering/annealing treatments. Bottom: general morphology of Au clusters on the TiO_2(110) surface (2.0 V, 2.0 nA). The evaporation rate was 0.083 ML min^{-1} and the Au coverage was 1.0 ML.

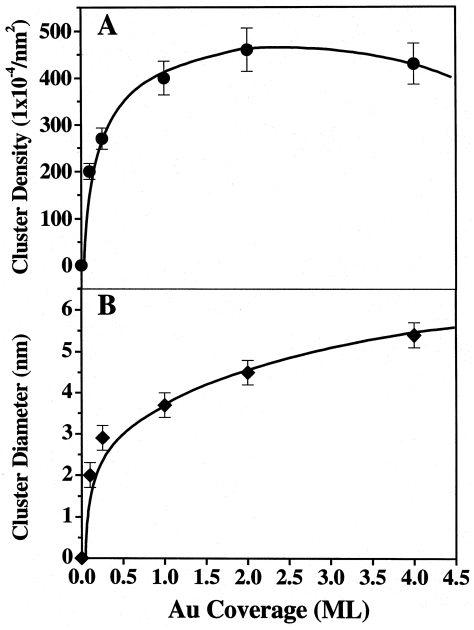

Fig. 2. Plots of the cluster density and cluster diameter vs. Au coverage on TiO_2(110).

increase in the average cluster volume. This correlation between Au coverage and Au cluster diameter demonstrates that vacuum deposition can produce a specific size range and shape of Au clusters, ideal for model catalyst studies.

3.2. Size-dependent CO oxidation over Au / TiO_2(110)

Recently, supported Au has received considerable attention because of its unusual catalytic properties. For example, Au, deposited as nanometer-sized clusters on reducible metal oxides such as TiO_2, exhibits extraordinary high activity for several reactions including low-temperature oxidation of CO, partial oxidation of hydrocarbons, hydrogenation of unsaturated hydrocarbons, and reduction of nitrogen oxides [55–75,82].

Reaction kinetics of CO oxidation has been carried out on various Au/TiO_2 catalysts. Fig. 3 shows the specific activity for CO oxidation in turnover frequency, {TOF, (product molecules) $\times$ (total Au atoms)$^{-1}$ $\times$ (s)$^{-1}$}, as a function of the average size of Au clusters supported on TiO_2. Two sets of data are shown in the graph, one for Au supported on planar TiO_2 [83] and the other for Au supported on high surface area TiO_2 [61]. The model Au/TiO_2 catalysts were prepared by vapor deposition of Au atoms onto planar TiO_2 thin films in UHV with the Au clusters characterized using STM. The high-surface-area Au/TiO_2 catalysts were synthesized by Bamwenda et al. [61] using a precipitation method, with the average cluster sizes monitored with TEM. These results show similarities in the structure sensitivity of CO oxidation with a maximum activity evident at $\sim$3.0-nm Au cluster size on both TiO_2 supports. The activity for both catalysts decreases with an increase in the Au cluster size. For each catalyst, the activity and selectivity of the supported Au clusters are markedly cluster-size dependent.

In order to address the structure sensitivity of CO oxidation over supported Au catalysts, the interaction of CO and O_2 with Au clusters of varying size supported on TiO_2 was investigated at elevated pressures. Fig. 4 shows the effects of a 10.00-Torr O_2 exposure to a 0.25-ML Au/TiO_2(110) surface [80]. Following deposition of Au at 300 K (Fig. 4A), Au clusters appear as bright images with a relatively

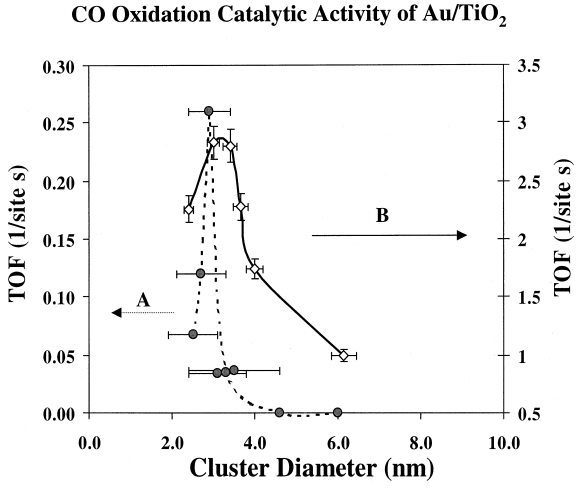

Fig. 3. CO oxidation turnover frequencies (TOFs) as a function of the Au cluster size supported on TiO_2. (A) The Au/TiO_2 catalysts were prepared by a precipitation method, and the averaged cluster sizes were measured by TEM, 300 K [61]. (B) The Au/TiO_2 catalysts were prepared by vapor-deposited Au atoms on planar TiO_2 films on Mo(100). The CO/O_2 mixture was 1:5 at a total pressure of 40 Torr, 350 K.

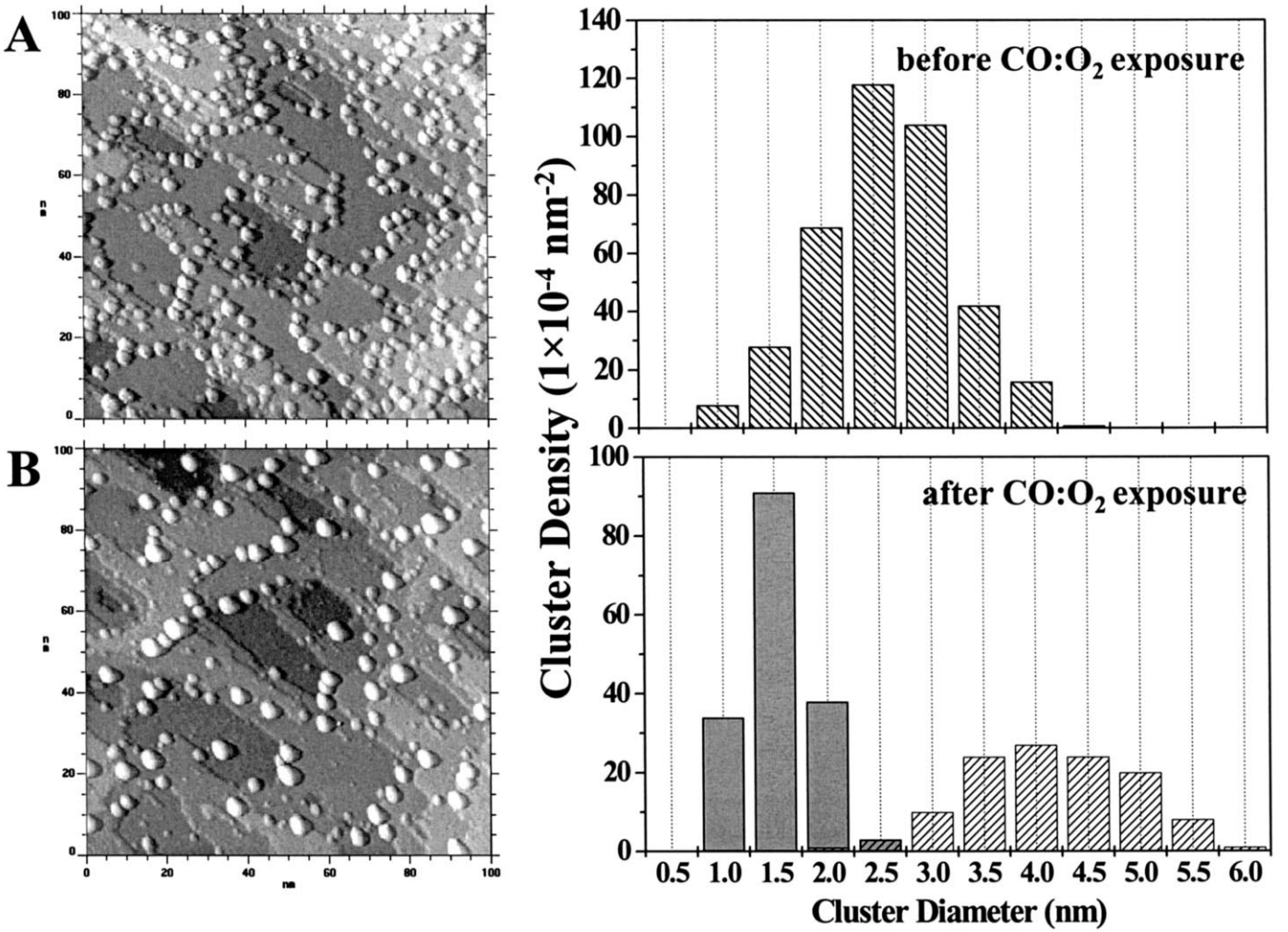

Fig. 4. Topographic STM images (100×100 nm^2, 2.0 V, 2.0 nA) and the corresponding size distributions of 0.25-ML Au clusters on the TiO_2(110) surface before and after 10.00-Torr CO/O_2 (2:1) exposure for 120 min at room temperature. (A) Fresh 0.25-ML Au deposited at room temperature. (B) 0.25-ML Au exposed to 10.00-Torr CO/O_2 (2:1) for 120 min at room temperature.

narrow size distribution. The clusters, with an average size of ~2.6 nm in diameter and ~0.7 nm in height, aggregate at the TiO_2(110) step edges. Following surface characterization, the Au/TiO_2(110) sample was transferred into the elevated-pressure cell and a CO/O_2 (2:1) gas mixture introduced at a total pressure of 10.00 Torr for 120 min at 300 K. Fig. 4B shows the effect of exposing the Au clusters to a 10.00-Torr CO/O_2 mixture. The number and density of the Au clusters are significantly reduced, with an increase in the average cluster size and height to ~3.6 and ~1.4 nm, respectively. In addition to the agglomeration of the Au clusters, extremely small clusters (~1.5 nm in diameter) are also formed. The size distribution of 0.25-ML Au/TiO_2(110) before and after the CO/O_2 exposure shows marked morphological changes. A bimodal distribution is apparent after the CO/O_2 exposure, i.e., some Au clusters increase in size while others become smaller.

XPS measurements before and after CO exposure show no change in the chemical composition of the Au clusters. The TiO_2(110) surface, on the other hand, became oxidized after the CO/O_2 exposure (Fig. 5). The small shoulder on the low-binding energy side of the XPS Ti 2p peak, corresponding to Ti^{3+} species, is absent after the 120-min CO/O_2 exposure at 300 K.

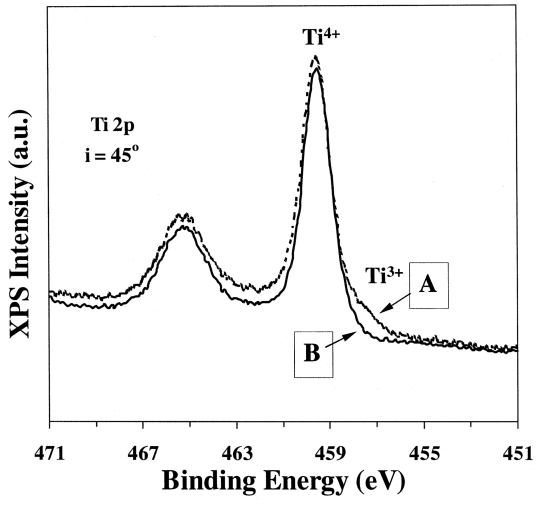

Fig. 5. XPS spectra for TiO_2 substrate before and after CO/O_2 exposure. (A) Slightly oxygen-deficient TiO_2 surface prepared by cycles of sputtering and annealing to 1100 K. (B) Fully oxidized TiO_2 surface after 10.00-Torr CO/O_2 exposure for 120 min at room temperature.

The influence of separate exposures of CO, O_2 and CO/O_2 at a total pressure of 10.00 Torr on the morphology and the size of Au clusters at 300 K is illustrated in Fig. 6. The adsorption of CO has no effect on the surface structure of the Au/TiO_2(110) (Fig. 6B). In addition, XPS measurements performed before and after the CO exposure confirm that the chemical composition of the Au/TiO_2(110) remained unchanged. STM images following O_2 and CO/O_2 exposures revealed a similar modification of the morphology of Au/TiO_2(110), i.e., the number and density of the Au clusters are greatly reduced and the average cluster size increased. Furthermore, oxidation of the TiO_2(110) surface was evident by XPS after the O_2 and CO/O_2 exposures (Fig. 5).

The identical structural and surface chemical changes upon exposure to O_2 and CO/O_2, with no detectable changes following an exposure to CO, show that the Au/TiO_2(110) surface exhibits an exceptionally high reactivity toward O_2 at 300 K that promotes the sintering of Au clusters. Although O_2 adsorption on atomically flat, metal single crystals of Au is a highly activated process with an extremely low sticking probability at 300 K [84], Au nanoclusters apparently can activate O_2 and produce atomically adsorbed oxygen [72].

These results provide compelling evidence that TiO_2(110)-supported Au nanoclusters are reactive toward O_2. Chemisorption of an atom or a molecule often promotes reorganization of the substrate atoms near the adsorption site. Depending on the strength of the surface–adsorbate bond, the surface can experience different degrees of restructuring, originating from either weak local relaxation or transport of surface atoms. Since the driving force is the minimization of the surface free energy, the formation of strong adsorbate–substrate bonds will consequently weaken the bonding of the substrate atoms. Metal clusters contain a relatively small number of atoms; thus, surface atoms can be easily influenced because of their low coordination number. Therefore, supported nanoclusters are extremely vulnerable to adsorbate-induced morphological changes.

Even though the TiO_2-supported Au catalysts exhibit a high activity for the low-temperature CO

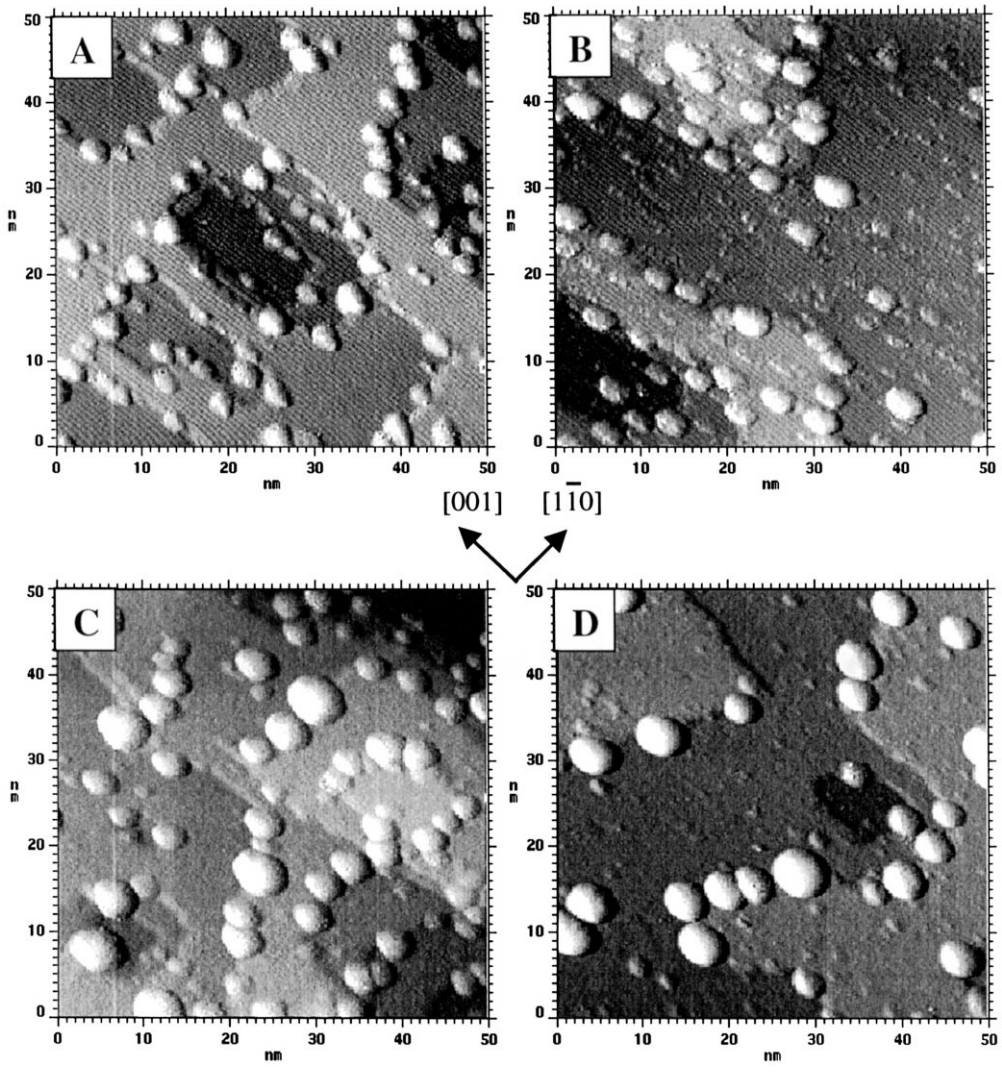

Fig. 6. A series of CCT STM images (2.0 V, 2.0 nA, 50×50 nm^2) of 0.25-ML Au/TiO_2(110). (A) Fresh 0.25-ML Au/TiO_2(110). (B) After 120 min exposure to 10.00-Torr CO at room temperature. (C) After 120 min exposure to 10.00-Torr O_2 at room temperature. (D) After 120 min exposure to 10.00-Torr CO/O_2 (2:1) at room temperature.

oxidation, the catalysts are often rapidly deactivated. This is illustrated in Fig. 7, where the CO conversion is plotted as a function of reaction time for CO oxidation at 300 K on 0.25-ML Au on TiO_2/Mo(100). The model Au/TiO_2 catalyst, which exhibits a high initial activity, deactivates after a CO/O_2 (1:5) reaction of $\sim$120 min at 40 Torr. Since a marked enhancement of the Au cluster size was observed for CO oxidation over 0.25-ML Au/TiO_2(110) at 300 K under similar elevated-pressure conditions, the deactivation is likely due to agglomeration of the Au clusters induced by interaction of O_2 with the Au clusters. The oxidation of the slightly oxygen deficient TiO_2 surface after the 120-min CO/O_2 exposure (see Fig. 5) likely lowers the activity of Au/TiO_2 even further because the fully oxidized stoichiometric TiO_2 surface has less affinity for O_2 at 300 K [79]. Oxidation of the TiO_2 surface during CO oxidation also provides direct evidence that the deactivation is not caused by encapsulation

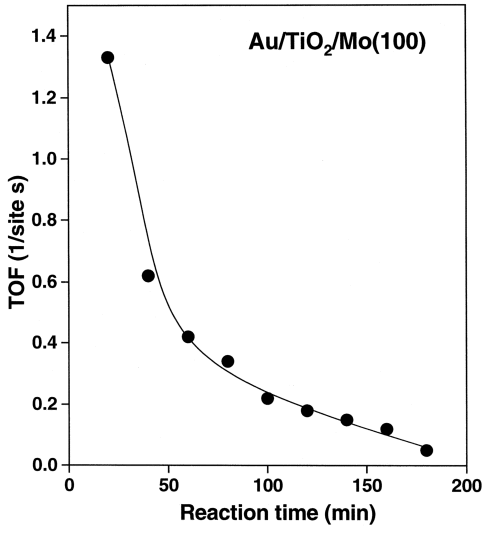

Fig. 7. The specific activity for CO conversion as a function of reaction time at 300 K on a model Au/TiO_2 /Mo(100) catalyst. The Au coverage was 0.25 ML, corresponding to an average cluster size of ~2.4 nm.

of Au clusters by reduced Ti suboxides as is the case for $Pt/TiO_2(110)$ [85].

The O_2-induced morphological changes are size dependent and consistent with the catalytic reactivity for CO oxidation since these were not observed for clusters larger than ~4.0 nm. Fig. 8 shows the surface morphologies of 1.6-ML $Au/TiO_2(110)$, with an initial average Au cluster size of ~4.2 nm, before and after O_2 exposure. The O_2 exposure clearly has little to no effect on the Au cluster size.

These results suggest that the catalytic properties of supported nanoclusters may deviate significantly from those of the bulk metal. The observed tailoring of the properties of small metal clusters by altering the cluster size could prove to be universal for a variety of metals, and should be useful in the design of nanostructured materials for catalytic applications. Furthermore, these results suggest that other metal nanocluster systems (such as Ag) could also be susceptible to O_2-induced morphological changes.

3.3. Oxygen-induced ripening of $Ag/TiO_2(110)$

The interaction of Ag with O_2 is of interest because of its use as an industrial catalyst for two technologically important oxidation reactions: ethylene oxidation to ethylene epoxide and methanol oxidation to formaldehyde [86–88]. To study the role that O_2 plays in cluster growth, Ag clusters, deposited onto a $TiO_2(110)$, were characterized using XPS and STM, before and after exposure to elevated pressures of O_2.

A 0.10-ML coverage of Ag on $TiO_2(110)$, corresponding to Ag clusters with an average size of ~3.0 nm, in contrast to Au clusters of similar size, remained unchanged in size and density following a 10.00-Torr O_2 exposure (not shown). Fig. 9A shows the surface morphology of 2.0-ML Ag deposited onto a $TiO_2(110)$ at room temperature [80]. Three-dimensional hemispherical Ag clusters with relatively homogeneous sizes were identified by STM to be on the average ~4.8 × 2.6 nm (diameter × height), corresponding to ~1900 atoms/cluster. The surface with 2.0-ML Ag was transferred into the elevated-pressure reactor and exposed to 10.00-Torr O_2 at room temperature for 120 min. The STM micrograph in Fig. 9 of the O_2-exposed 2.0-ML $Ag/TiO_2(110)$ surface shows that the O_2 exposure dramatically influences the cluster sizes, analogously to Au clusters exposed to O_2. A bimodal Ag cluster size distribution is evident, some clusters increasing in size while others become smaller. A significant increase (5–15%) in cluster density was also observed, indicating that redispersion occurs as well.

Size distributions measured from the STM images of Ag clusters before and after high-pressure O_2 exposure are shown in Fig. 9. Initially, the Ag clusters exhibited a uniform size distribution from 2.0 to 6.5 nm with a maximum diameter of ~5.0 nm. However, following an O_2 exposure, a bimodal size distribution was evident with one size domain from 1.0 to 5.0 nm and a second from 5.0 to 11 nm. The smaller clusters in the range 1.0–5.0 nm have a higher density and narrower size distribution, with an average Ag cluster size of ~3.0 × ~1.1 nm (~260 atoms). The larger clusters have a lower cluster density and a broader size distribution, averaging ~6.7 × ~3.1 nm (~4200 Ag atoms per cluster). XPS indicates a constant Ag $3d_{5/2}$ binding energy following an O_2 exposure, consistent with the XPS results for technical Ag catalysts [88]. It is noteworthy that the total cluster volume before and after O_2 exposure determined by STM agrees within 10%.

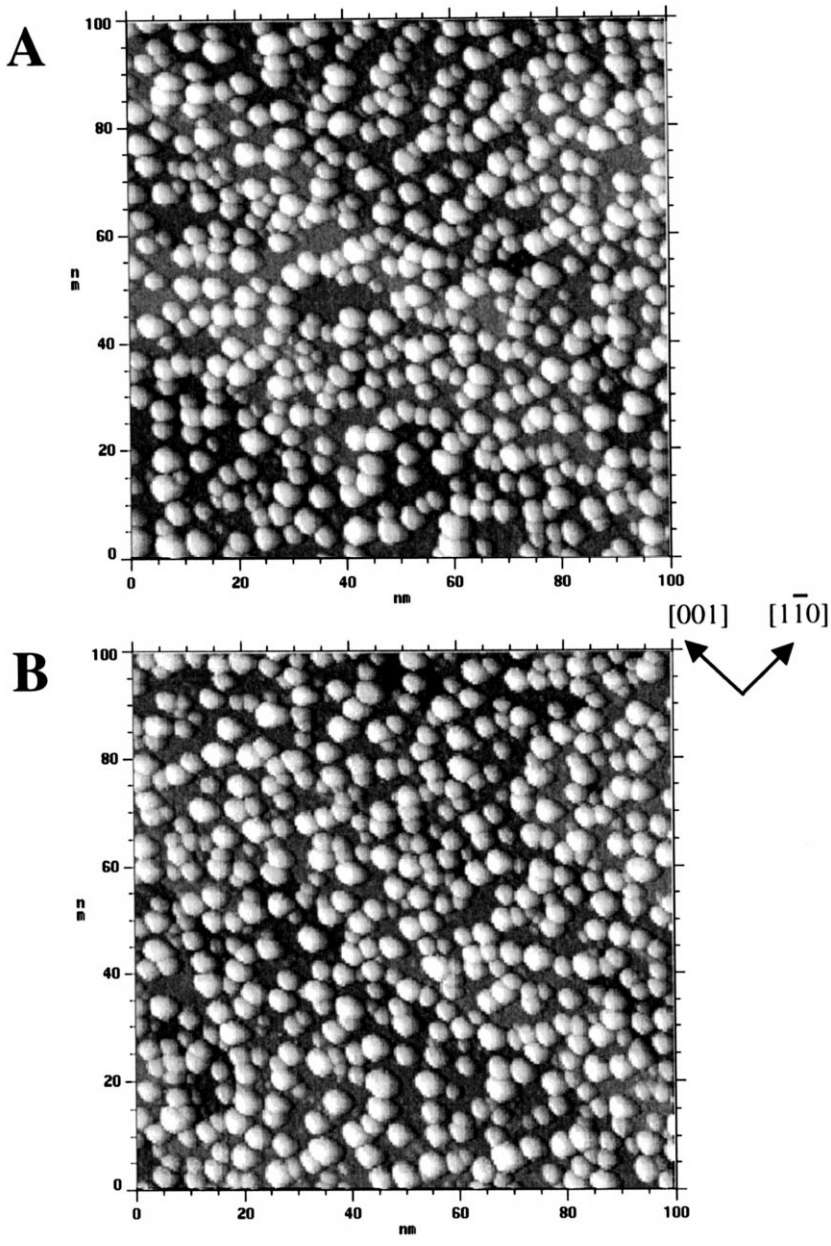

Fig. 8. Topographic STM images (100×100 nm^2, 2.5 V, 0.3 nA) of 1.60-ML Au clusters on the TiO_2(110). (A) Fresh 1.60-ML Au deposited at room temperature. (B) 1.60-ML Au exposed to 10.00-Torr O_2 for 120 min at room temperature.

Similar O_2-induced ripening effects for Au and Ag with similar cluster size distribution are apparent, suggesting an intrinsic cluster-size dependency with respect to O_2 for Au and Ag. This behavior has been observed for other metals and other structure-sensitive reactions. For example, for ethane hydrogenolysis over supported Ni catalysts, catalytic activity increases with increasing cluster size, reaching a maximum at a cluster size of $\sim$2.5 nm [89]. These size dependencies can be attributed to intrinsic clus-

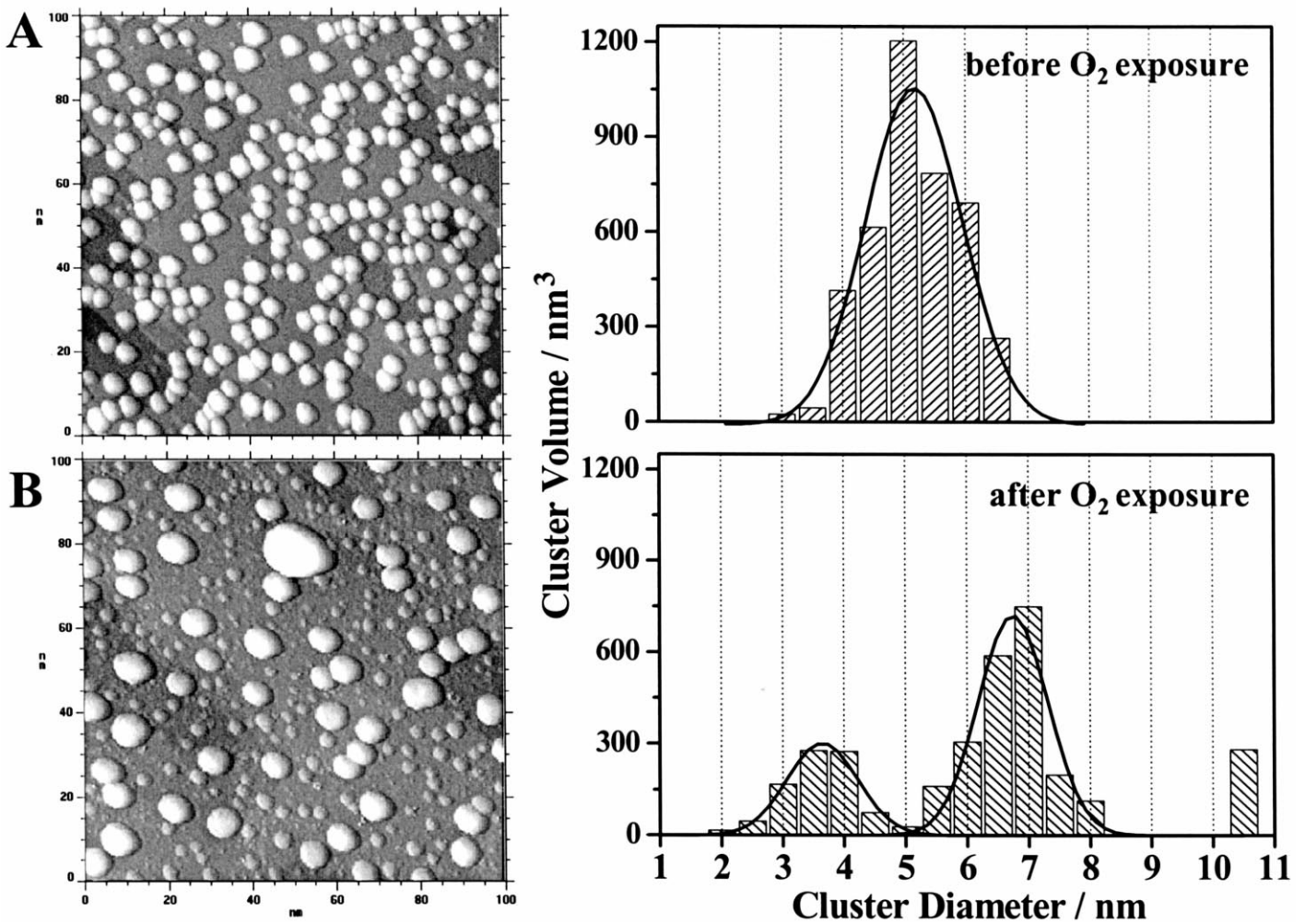

Fig. 9. Topographic STM images (100×100 nm^2, 2.0 V, 1.0 nA) and the corresponding size distributions of 2.0-ML Ag clusters on the $TiO_2(110)$ surface before and after 10.00-Torr O_2 exposure for 120 min at room temperature. A bimodal size distribution results after the exposure. (A) Fresh 2.0-ML Ag on a clean $TiO_2(110)$. (B) 2.0-ML $Ag/TiO_2(110)$ exposed to 10.00-Torr O_2 for 120 min.

ter-size effects resulting from changes in the average atom-coordination number and/or a metal–support interaction.

3.4. Ostwald ripening process

Since oxide-supported metal catalysts typically are exposed to elevated O_2 pressures, an analysis of O_2-induced morphological changes is relevant. In general, cluster growth of supported metal catalysts can proceed via two processes. First, clusters can migrate along the surface, collide with other clusters, and coalescence. Second, cluster growth can occur by intercluster transport, or Ostwald ripening, driven by capillary action. In the latter case, the reduction of the total surface free energy by intercluster transport occurs such that certain clusters grow larger at the expense of other clusters [90]. The bimodal size distribution found for Au and Ag subsequent to O_2 exposure then is most consistent with Ostwald ripening.

The Ostwald ripening process is illustrated in Fig. 10. Intercluster transport of atomic (or molecular) species can occur by either surface diffusion along the substrate or via vapor-phase transport. Using Ag as an example, under vacuum or reducing conditions, the transport between Ag clusters can only occur via free metallic Ag atoms, driven by the Ag vapor pressure. The Ag vapor pressure depends exponentially on the energy required to break Ag−Ag metal bonds and to transfer an Ag atom to the vapor phase (i.e., the sublimation energy $\Delta H_{\mathrm{subl}}(\mathrm{Ag}) \approx 285$ kJ mol^{-1}). The magnitude of this barrier suggests that intercluster transport by free Ag toms should be relatively slow at room temperature, consistent with the STM images indicating that Ag clusters are generally stable in UHV conditions.

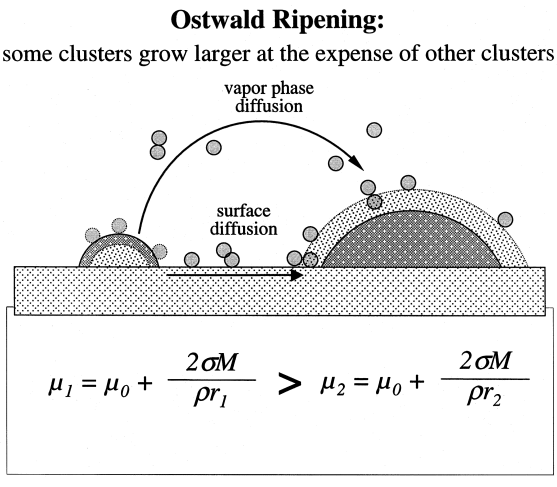

Fig. 10. Schematic illustration of the Ostwald ripening process: atomic intercluster transport leads to a bimodal size distribution.

In an oxidizing environment, the situation is quite different. For example, Wynblatt [91] showed that growth of Pt particles in an O_2 environment is via the formation of volatile PtO_2. Platinum oxide has a lower sublimation energy than platinum metal and therefore serves as an intermediate by which intercluster transport can occur. Unfortunately, to the best of our knowledge, no vapor pressure or sublimation energy data are available for silver oxide (Ag_2O), making it difficult to compare Ag directly with Pt. However, it can be shown that the formation of Ag_2O from Ag particles in 10.00-Torr O_2 is at least thermodynamically favorable and thus may account for the intercluster transport observed.

Thermodynamically, Ag can form Ag_2O by reacting with oxygen at room temperature. This can be illustrated by considering the following simple reaction:

$$2\mathrm{Ag(s)} + 1/2\mathrm{O_2(g)} \rightarrow \mathrm{Ag_2O(s)} \quad (1)$$

that has a negative standard free energy of formation of Ag_2O ($\Delta G_{298} = -11.2$ kJ mol^{-1}) at room temperature. The equilibrium constant K_{P} for the above reaction can be expressed as:

$$K_{\mathrm{P}} = \frac{a_{\mathrm{P}}}{a_{\mathrm{Ag}}^2 P_{\mathrm{O_2}}^{1/2}} \quad (2)$$

where a_{P} and a_{Ag} are the activities of Ag_2O and Ag, respectively (both values are unity), and $P_{\mathrm{O_2}}$ is the equilibrium partial pressure of oxygen. Substitution of K_{P} into the standard ΔG equation yields:

$$\Delta G_T = 1/2\, RT \ln P_{\mathrm{O_2}} \quad (3)$$

where T is the absolute temperature and R is the universal gas constant. Ag oxidation can only occur if the partial pressure of O_2 is higher than the $P_{\mathrm{O_2}}$ value in Eq. (3) for $T = 298$ K. By substituting $\Delta G_{298} = -11.2$ kJ mol^{-1} into Eq. (3), the equilibrium oxygen partial pressure $P_{\mathrm{O_2}}$ is predicted to be

1.23×10^{-4} atm (0.094 Torr). Since the partial pressure (10.00 Torr) is higher than the equilibrium oxygen partial pressure at 300 K, the oxidation of bulk Ag should be thermodynamically favorable.

An additional effect that must be considered is the influence of the Ag-cluster curvature on the free energy. The decrement Δg in free energy due to cluster curvature is given by:

$$\Delta g = \frac{2\sigma M}{\rho r} \tag{4}$$

where σ is the surface energy, M is the atomic weight, ρ is the density and r is the cluster-curvature radius [92]. At room temperature, taking $\sigma =$ 1400 erg cm^{-2} [93] and $\rho = 10.5$ g cm^{-3}, $\Delta G_{298}(r)$, the standard free energy of formation of Ag_2O for Ag clusters with curvature radius r (in nanometers), is given by:

$$\Delta G_{298}(r) = \Delta G_{298} - \Delta g$$
$$= -11.2 - 28.8/r \ (\mathrm{kJ\,mol^{-1}}). \tag{5}$$

For an average cluster diameter of 5.0 nm ($r = 2.5$ nm), the value of $\Delta G_{298}(r)$ is doubled ($\Delta G_{298}(r) = -22.7$ kJ mol^{-1}). As the cluster size decreases further to 3.0 nm ($r = 1.5$ nm), the absolute $|\Delta G_{298}(r)|$ value increases by a factor of 1.7. Therefore, the driving force for oxidation of Ag nanoclusters is increased significantly at room temperature, taking into account the cluster curvature.

Obviously, specific sizes of Ag clusters are more reactive to O_2 molecules than others, thus, certain sizes of Ag clusters undergo Ostwald ripening more rapidly. Other sizes of Ag clusters undergo this process more slowly due to their low reactivity to O_2. Therefore, the size-dependent bimodal distribution is a result of Ostwald ripening. A similar Ostwald ripening process should be expected for Au clusters as well. However, because the necessary thermodynamic data for AuO_x are not available, an analogous calculation cannot be made for Au clusters.

While this analysis shows that Ag_2O formation from Ag and O_2 is possible at room temperature, little can be concluded regarding the rate of Ag_2O formation. However, time-dependent studies of the O_2 exposure can at least suggest relative rates of the Ostwald ripening process. Fig. 11 shows STM images of 2.0-ML $Ag/TiO_2(110)$ after exposure to 10.00-Torr O_2 for 10 and 60 min, respectively. For a 10-min exposure, Ostwald ripening is apparent, although the bimodal distribution is not as clear as in the 60-min exposure. Furthermore, little difference in the morphologies of $Ag/TiO_2(110)$ is evident between a 60- and a 120-min O_2 exposure, suggesting that Ostwald ripening is rapid and complete in 1–2 h. These Ostwald ripening kinetics are consistent with the deactivation times typically found for Au catalysts during the CO oxidation (see Fig. 7).

3.5. Effect of substrate on the ripening process

The substrate, and its influence on cluster ripening, is an important consideration. The oxide support often is not simply a mechanical support for the metal clusters but can influence the electronic properties of the metal clusters. In certain cases, the support can migrate onto the clusters as occurs in the so-called strong metal–support interaction (SMSI) [94]. As has been shown, a vacuum anneal leads to a slightly oxygen-deficient TiO_2 surface. After O_2 exposure, the TiO_2 substrate becomes fully oxidized and the metal clusters ripen. O_2 must be strongly adsorbed onto the oxygen vacancies or defects of the substrate and could play an important role in the Ostwald ripening process. Therefore, if Ag clusters were prepared on a fully oxidized $TiO_2(110)$ and similarly exposed to O_2, the coverage of chemisorbed O_2 on oxidized $TiO_2(110)$ should be significantly less than that on the reduced surface.

Fig. 12 demonstrates the influence of the substrate on the behavior of Ag clusters with O_2 exposure. Image A shows Ostwald ripening for Ag clusters supported on a slightly oxygen-deficient $TiO_2(110)$ surface exposed to 10.00-Torr O_2. Some Ag clusters grow to 15 nm in diameter and 7 nm in height ($\sim$47,000 atoms). The second support is a fully oxidized $TiO_2(110)$, prepared by exposing a clean TiO_2 substrate (slightly oxygen deficient) to 10.00-Torr O_2 for 120 min until fully oxidized. Ag clusters were then vapor-deposited onto this surface. However, the corresponding O_2 exposure on this sample revealed a less-pronounced Ostwald ripening process, as shown in Fig. 12B. The largest Ag clusters were only $\sim$7.0–8.0 nm in diameter. These data

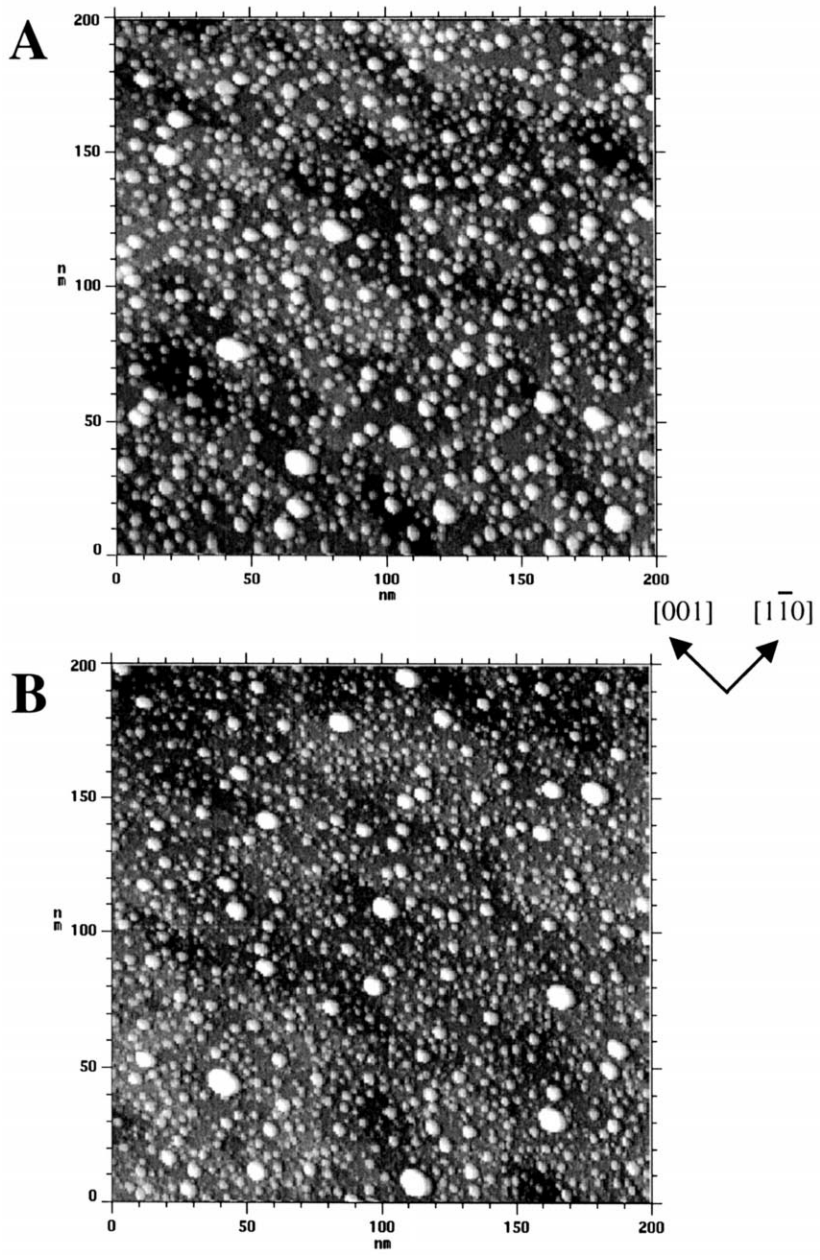

Fig. 11. Effects of O_2 exposure time on 2.0-ML $Ag/TiO_2(110)$: (200×200 nm^2, 2.0 V, 1.0 nA). (A) 2.0-ML $Ag/TiO_2(110)$ exposed to 10.00-Torr O_2 for 10 min. (B) 2.0-ML $Ag/TiO_2(110)$ exposed to 10.00-Torr O_2 for 60 min.

showed that the substrate plays an important factor in the ripening process. During the exposure, O_2 molecules were adsorbed onto the Ag clusters as well as onto surface vacancies or defects. This chemisorbed O_2 species helped to facilitate the intercluster transport of Ag atoms along the surface. A fully oxidized support with less surface vacancies or defects should adsorb less O_2. Therefore, the pathway for intercluster transport via the substrate surface is inhibited. Surface defects or vacancies, there-

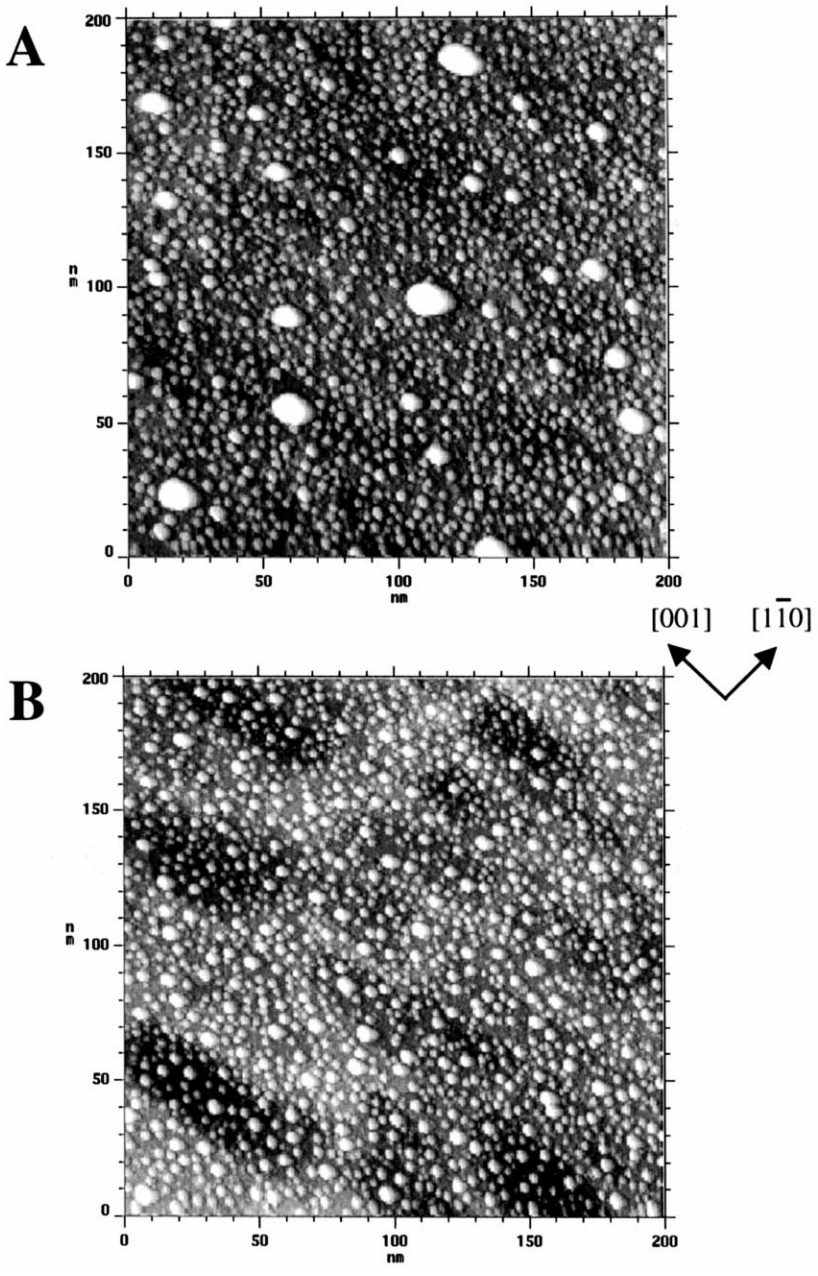

Fig. 12. Inhibition of cluster ripening (200×200 nm^2, 2.0 V, 1.0 nA). (A) 2.0-ML Ag/TiO_2(110) exposed to 10.00-Torr O_2 for 120 min. (B) 2.0-ML Ag/fully oxidized TiO_2(110) exposed to 10.00-Torr O_2 for 120 min.

fore, play an important role in promoting the ripening process.

Varying the oxide support for the Ag clusters can further test the effect of the substrate on ripening. First, an Al_2O_3 thin film on Re(0001) was prepared as described previously. Compared to TiO_2, Al_2O_3 is irreducible and unreconstructed, and no SMSI has been found for metal–Al_2O_3 systems. Subsequently,

Ag clusters were then vapor-deposited onto the thin film followed by a 10.00-Torr O_2 exposure.

A series of STM micrographs of Ag/Al_2O_3 following an O_2 exposure are presented in Fig. 13. As a reference, image A is an STM image of a 2.0-ML Ag deposit on a clean $TiO_2(110)$ surface, showing a homogeneous Ag-cluster size distribution. Image B is an STM image of the same coverage of Ag deposited onto an Al_2O_3 thin film. The Ag clusters are slightly larger, and have a smaller density. The Ag clusters on Al_2O_3 were then exposed to 10.00-Torr O_2 in an elevated-pressure cell for 120 min at 300 K, following the same treatment used for $Ag/TiO_2(110)$. Image C revealed little change after this exposure. However, when the O_2 pressure was further increased to 1000 Torr, the Ag cluster obvi-

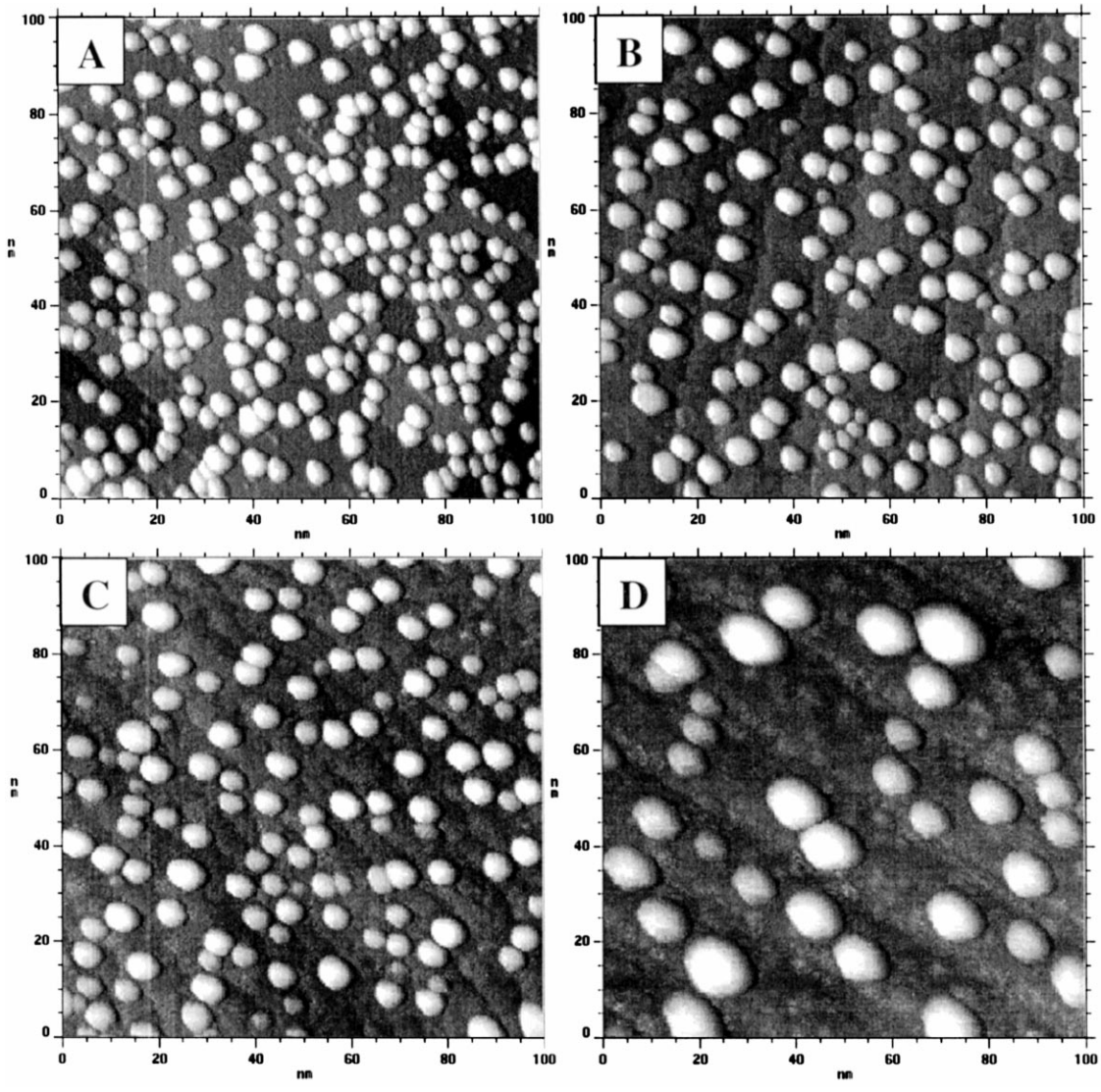

Fig. 13. Effects of O_2 exposures on 2.0-ML $Ag/Al_2O_3/Re(0001)$. (A) Fresh 2.0-ML $Ag/TiO_2(110)$, 2.0 V, 1.0 nA. (B) Fresh 2.0-ML $Ag/Al_2O_3/Re(0001)$, 2.0 V, 0.26 nA. (C) 2.0-ML $Ag/Al_2O_3/Re(0001)$ exposed to 10-Torr O_2 for 120 min. (D) 2.0-ML $Ag/Al_2O_3/Re(0001)$ exposed to 1000-Torr O_2 for 120 min.

ously ripened, as illustrated in image D. These results confirm that Ag clusters on Al_2O_3 are more stable compared to TiO_2(110). The relatively defect-free Al_2O_3 support reduces the reactivity of metal clusters toward O_2 and inhibits cluster ripening.

4. Conclusions

Insight into the atomic-level surface chemistry of metals on oxide surfaces is vital to understanding heterogeneous catalysis. The work summarized is based on the use of planar model catalysts prepared in UHV to simulate the corresponding "real world" catalysts. The physical and chemical properties of supported metal clusters have been explored and the reasons for the extraordinary high activity of CO oxidation on Au/TiO_2 have been investigated. A correlation has been found between the cluster size and the catalytic activity of Au/TiO_2. Similar O_2-induced morphological changes for Au and Ag clusters were observed subsequent to an elevated-pressure O_2 exposure. Ostwald ripening, where certain clusters grow at the expense of other clusters, leads to a bimodal cluster size distribution. Volatile oxide species are formed at elevated oxygen pressures and accelerate the intercluster atom transport. The substrate also plays an important role in this ripening process in that a surface with enhanced defects or oxygen vacancies facilitates the ripening process.

Acknowledgements

We acknowledge with pleasure the support of this work by the Department of Energy, Office of Basic Energy Sciences, Division of Chemical Sciences, the Robert A. Welch Foundation, and the Dow Chemical.

References

[1] C.T. Campbell, Surf. Sci. Rep. 27 (1997) 1.
[2] D.R. Rainer, C. Xu, D.W. Goodman, J. Mol. Catal. A: Chem. 119 (1997) 307.
[3] C.R. Henry, Surf. Sci. Rep. 31 (1998) 231.
[4] A. Fujishima, K. Honda, Nature 37 (1972) 238.
[5] H. Onishi, K. Fukui, Y. Iwasawa, Bull. Chem. Soc. Jpn. 68 (1995) 2447.
[6] H. Onishi, Y. Iwasawa, Chem. Phys. Lett. 226 (1994) 111.
[7] H. Onishi, Y. Iwasawa, Langmuir 10 (1994) 4414.
[8] U. Diebold, J.F. Anderson, K. Ng, D. Vanderbilt, Phys. Rev. Lett. 77 (1996) 1322.
[9] M. Sander, T. Engel, Surf. Sci. Lett. 302 (1994) L263.
[10] A. Szabo, T. Engel, Surf. Sci. 329 (1995) 241.
[11] Y. Iwasawa, Surf. Sci. 402–404 (1998) 8.
[12] U. Diebold, J. Lehman, T. Mahmoud, M. Kuhn, G. Leonardelli, W. Hebenstreit, M. Schmid, P. Varga, Surf. Sci. 411 (1998) 137.
[13] G.S. Rohrer, V.E. Henrich, D.A. Bonnell, Surf. Sci. 278 (1992) 146.
[14] T. Engel, Langmuir 12 (1996) 1428.
[15] H. Onishi, Y. Iwasawa, Surf. Sci. 357–358 (1996) 773.
[16] P.W. Murray, N.G. Condon, G. Thornton, Phys. Rev. B 51 (1995) 10989.
[17] D. Novak, E. Garfunkel, T. Gustafsson, Phys. Rev. B 50 (1994) 5000.
[18] F.M. Leibsle, P.W. Murray, N.G. Condon, G. Thornton, J. Phys. D: Appl. Phys. 30 (1997) 741.
[19] H. Onishi, Y. Yamaguchi, K. Fukui, Y. Iwasawa, J. Phys. Chem. 100 (1996) 9582.
[20] K. Ng, D. Vanderbilt, Phys. Rev. B 56 (1997) 10544.
[21] Q. Zhong, J.M. Vohs, D.A. Bonnell, Surf. Sci. 274 (1992) 35.
[22] Q. Guo, I.D. Cocks, E.M. Williams, J. Phys. D: Appl. Phys. 31 (1998) 2231.
[23] I.D. Cocks, Q. Guo, E.M. Williams, Surf. Sci. 390 (1997) 119.
[24] H. Sugimura, T. Uchida, N. Kitamura, H. Masuhara, J. Phys. Chem. 98 (1994) 4352.
[25] O. Gülseren, R. James, D.W. Bullett, Surf. Sci. 377–379 (1997) 150.
[26] S. Suzuki, H. Onishi, T. Sasaki, K. Fukui, Y. Iwasawa, Catal. Lett. 54 (1998) 177.
[27] R.E. Tanner, M.R. Castell, G.A.D. Briggs, Surf. Sci. 412/413 (1998) 672.
[28] H. Raza, C.L. Pang, S.A. Haycock, G. Thornton, Phys. Rev. Lett. 82 (26) (1999) 5265.
[29] R.G. Egdell, F.H. Jones, J. Mater. Chem. 8 (3) (1998) 469.
[30] R.A. Bennett, S. Poulston, P. Stone, M. Bowker, Phys. Rev. B 59 (15) (1999) 10341.
[31] V.E. Henrich, P.A. Cox, The Surface Science of Metal Oxides, Cambridge Univ. Press, Cambridge, 1994.
[32] J.M. Pan, B.L. Maschhoff, U. Diebold, T.E. Madey, J. Vac. Sci. Technol., A 10 (1992) 2470.
[33] K.F. Ferris, L.Q. Wang, J. Vac. Sci. Technol., A 16 (1998) 956.
[34] L.Q. Wang, K.F. Ferris, J. Vac. Sci. Technol., A 16 (1998) 3034.
[35] L.Q. Wang, K.F. Ferris, A.N. Shultz, D.R. Baer, M.H. Engelhard, Surf. Sci. 380 (1997) 352.
[36] M.A. Barteau, Chem. Rev. 96 (1996) 1413.

[37] I.D. Cocks, Q. Guo, R. Patel, E.M. Williams, E. Roman, J.L. de Segovia, Surf. Sci. 377–379 (1997) 135.
[38] R.L. Kurtz, R. Stockbauer, T.E. Madey, Surf. Sci. 218 (1989) 178.
[39] W. Göpel, J.A. Anderson, D. Frankel, M. Jaehnig, K. Phillips, J.A. Schäfer, G. Rocker, Surf. Sci. 139 (1984) 333.
[40] Y. Yanagisawa, Y. Ota, Surf. Sci. Lett. 254 (1991) L433.
[41] W. Göpel, G. Rocker, R. Feierabend, Phys. Rev. B 28 (1983) 3427.
[42] G. Lu, A. Linsebigler, J.T. Yates Jr., J. Phys. Chem. 98 (1994) 11733.
[43] A. Linsebigler, G. Lu, J.T. Yates Jr., J. Chem. Phys. 103 (1995) 9438.
[44] K. Hadjiivanov, J. Lamotte, J.C. Lavalley, Langmuir 13 (1997) 3374.
[45] D.D. Beck, J.M. White, C.T. Ratcliffe, J. Phys. Chem. 90 (1986) 3123.
[46] D.D. Beck, J.M. White, C.T. Ratcliffe, J. Phys. Chem. 90 (1986) 3132.
[47] D.D. Beck, J.M. White, C.T. Ratcliffe, J. Phys. Chem. 90 (1986) 3137.
[48] A. Berkó, G. Ménesi, F. Solymosi, Surf. Sci. 372 (1997) 202.
[49] A. Berkó, F. Solymosi, Surf. Sci. 400 (1998) 281.
[50] A. Berkó, G. Ménesi, F. Solymosi, J. Phys. Chem. 100 (1996) 17732.
[51] A. Berkó, F. Solymosi, J. Catal. 183 (1999) 91.
[52] A. Berkó, F. Solymosi, Surf. Sci. 411 (1998) L900.
[53] M. Che, C.O. Bennett, Adv. Catal. 36 (1989) 55.
[54] E.D. Park, J.S. Lee, J. Catal. 186 (1999) 1.
[55] F. Boccuzzi, A. Chiorino, S. Tsubota, M. Haruta, J. Phys. Chem. 100 (1996) 3625.
[56] S. Minicò, S. Scirè, C. Crisafulli, A.M. Visco, S. Galvagno, Catal. Lett. 47 (1997) 273.
[57] M.A.P. Dekkers, M.J. Lippits, B.E. Nieuwenhuys, Catal. Lett. 56 (1998) 195.
[58] T. Hayashi, K. Tanaka, M. Haruta, J. Catal. 178 (1998) 566.
[59] M. Haruta, Catal. Surv. Jpn. 1 (1997) 61.
[60] S. Tsubota, T. Nakamura, K. Tanaka, M. Haruta, Catal. Lett. 56 (1998) 131.
[61] G.R. Bamwenda, S. Tsubota, T. Nakamura, M. Haruta, Catal. Lett. 44 (1997) 83.
[62] M. Okumura, S. Nakamura, S. Tsubota, T. Nakamura, M. Azuma, M. Haruta, Catal. Lett. 51 (1998) 53.
[63] M. Haruta, Catal. Today 36 (1997) 153.
[64] S.D. Lin, M. Bollinger, M.A. Vannice, Catal. Lett. 17 (1993) 245.
[65] K. Fukushima, G.H. Takaoka, J. Matsuo, I. Yamada, Jpn. J. Appl. Phys. 36 (1997) 813.
[66] N.W. Cant, N.J. Ossipoff, Catal. Today 36 (1997) 125.
[67] Z.M. Liu, M.A. Vannice, Catal. Lett. 43 (1997) 51.
[68] M.A. Bollinger, M.A. Vannice, Appl. Catal., B 8 (1996) 417.
[69] H. Sakurai, M. Haruta, Appl. Catal., A 127 (1995) 93.
[70] M. Haruta, N. Yamada, T. Kobayashi, S. Iijima, J. Catal. 115 (1989) 301.
[71] M. Haruta, S. Tsubota, T. Kobayashi, H. Kageyama, M.J. Genet, B. Delmon, J. Catal. 144 (1993) 175.
[72] Y. Iizuka, H. Fujiki, N. Yamauchi, T. Chijiiwa, S. Arai, S. Tsubota, M. Haruta, Catal. Today 36 (1997) 115.
[73] Y. Yuan, K. Asakura, H. Wan, K. Tsai, Y. Iwasawa, Catal. Lett. 42 (1996) 15.
[74] S. Tsubota, D.A.H. Cunningham, Y. Bando, M. Haruta, Preparation of Catalysts VI, Elsevier, Amsterdam, 1995, pp. 227–235.
[75] J.D. Grunwaldt, A. Baiker, J. Phys. Chem. B 103 (1999) 1002.
[76] C. Xu, X. Lai, G.W. Zajac, D.W. Goodman, Phys. Rev. B 56 (1997) 13464.
[77] X. Lai, T.P. St. Clair, M. Valden, D.W. Goodman, Prog. Surf. Sci. 59 (1998) 25.
[78] R.C. Weast, M.J. Astle, W.H. Beyer (Eds.), Handbook of Chemistry and Physics, 68th edn., CRC Press, Boca Raton, 1988, p. E-395.
[79] C. Xu, W.S. Oh, G. Liu, D.Y. Kim, D.W. Goodman, J. Vac. Sci. Technol., A 15 (1997) 1261.
[80] X. Lai, T.P. St. Clair, D.W. Goodman, Faraday Discuss. 114 (1999) 279.
[81] C. Xu, X. Lai, D.W. Goodman, Faraday Discuss. 105 (1996) 247.
[82] M. Valden, X. Lai, D.W. Goodman, Science 281 (1998) 1647.
[83] M. Valden, S. Pak, X. Lai, D.W. Goodman, Catal. Lett. 56 (1998) 7.
[84] N.D.S. Canning, D. Outka, R.J. Madix, Surfactant Sci. Ser. 141 (1984) 240.
[85] F. Pesty, H.P. Steinrück, T.E. Madey, Surf. Sci. 339 (1995) 83.
[86] S. Cheng, A. Clearfield, J. Catal. 94 (1985) 455.
[87] V.I. Bukhtiyarov, I.P. Prosvirin, R.I. Kvon, S.N. Goncharova, B.S. Bal'zhinimaev, J. Chem. Soc., Faraday Trans. 93 (13) (1997) 2323.
[88] V.I. Bukhitiyarov, A.I. Boronin, I.P. Prosvirin, V.I. Savchenko, J. Catal. 150 (1994) 268.
[89] K. Coulter, X. Xu, D.W. Goodman, J. Phys. Chem. 98 (1994) 1245.
[90] P. Wynblatt, R.A. Dalla Betta, N.A. Gjostein, in: E. Drauglis, R.I. Jaffee (Eds.), The Physical Basis for Heterogeneous Catalysis, Plenum, New York, 1975, p. 501.
[91] P. Wynblatt, Acta Metall. 24 (1976) 1175.
[92] J.D. Verhoeven, Fundamentals of Physical Metallurgy, Wiley, New York, 1975, p. 169.
[93] J.D. Verhoeven, Fundamentals of Physical Metallurgy, Wiley, New York, 1975, p. 202.
[94] R. Persaud, T.E. Madey, in: D.A. King, D.P. Woodruff (Eds.), The Chemical Physics of Solid Surfaces and Heterogeneous Catalysis vol. 8 Elsevier, Amsterdam, 1997, p. 407.